Global chromatin compaction limits the strength of the DNA damage response

Matilde Murga,[1] Isabel Jaco,[2] Yuhong Fan,[3] Rebeca Soria,[1] Barbara Martinez-Pastor,[1] Myriam Cuadrado,[1] Seung-Min Yang,[3] Maria A. Blasco,[2] Arthur I. Skoultchi,[3] and Oscar Fernandez-Capetillo[1]

[1]Genomic Instability Group and [2]Telomeres and Telomerase Group, Molecular Oncology Programme, Spanish National Cancer Center, Madrid 28029, Spain
[3]Department of Cell Biology, Albert Einstein College of Medicine, Bronx, NY 10467

In response to DNA damage, chromatin undergoes a global decondensation process that has been proposed to facilitate genome surveillance. However, the impact that chromatin compaction has on the DNA damage response (DDR) has not directly been tested and thus remains speculative. We apply two independent approaches (one based on murine embryonic stem cells with reduced amounts of the linker histone H1 and the second making use of histone deacetylase inhibitors) to show that the strength of the DDR is amplified in the context of "open" chromatin. H1-depleted cells are hyperresistant to DNA damage and present hypersensitive checkpoints, phenotypes that we show are explained by an increase in the amount of signaling generated at each DNA break. Furthermore, the decrease in H1 leads to a general increase in telomere length, an as of yet unrecognized role for H1 in the regulation of chromosome structure. We propose that slight differences in the epigenetic configuration might account for the cell-to-cell variation in the strength of the DDR observed when groups of cells are challenged with DNA breaks.

Introduction

The role of chromatin in the responses to DNA damage is currently the focus of intense study. On the one hand, the local modification or remodeling of histones at sites of DNA double-strand breaks (DSBs), such as the phosphorylation of the histone H2A variant H2AX (Rogakou et al., 1998), has led to the proposal of a DNA repair–specific "histone code" (Fernandez-Capetillo et al., 2004) that, through combinatorial histone modifications, might coordinate the signaling and repair of the lesions. On the other hand, and besides the local changes at the break site, work done two decades ago showed that the presence of DSBs triggers a global chromatin relaxation process (Takahashi and Kaneko, 1985). The interest in this phenomenon has now revived because of recent data showing that this DSB-induced chromatin decondensation is actively regulated by the DNA damage response (DDR; Ziv et al., 2006). Likewise, a global increase in chromatin accessibility has been reported in response to UV damage, which is mediated by p53 and Gadd45a proteins (Carrier et al., 1999; Rubbi and Milner, 2003). These observations led the authors to propose that the relaxation of chromatin might facilitate genomic surveillance by enabling faster access of DDR factors to the DSBs. However, the precise effect that the overall compaction status of the chromatin exerts on the access, signaling, and repair of DNA damage is not known and remains a central issue for our understanding of the DDR.

One of the main factors involved in high-order chromatin compaction is the linker histone H1. Through its binding to the internucleosomal linker DNA, in vitro data showed that H1 can help stabilize DNA at the nucleosomal linker DNA interface, thus favoring the refolding of arrays of nucleosome core particles into more compact structures (for review see Woodcock et al., 2006). The existing in vivo knowledge comes from the selective elimination of linker histones in several organisms. Attempts to deplete H1 protein in mice led to embryonic lethality when total H1 levels were reduced to ~50% of the wild-type level by inactivating three of the six somatic H1 genes (H1c, H1d, and H1e; Fan et al., 2003). However, triple-knockout murine embryonic stem (ES) cell lines ($H1^{50}$) also containing half

Correspondence to O. Fernandez-Capetillo: ofernandez@cnio.es

Y. Fan's present address is the School of Biology and the Petit Institute of Bioengineering and Bioscience, Georgia Institute of Technology, Atlanta, GA 30332.

Abbreviations used in this paper: ATM, ataxia telangiectasia mutated; ATR, ATM and Rad3 related; BP1, binding protein 1; Chk1, chaperoning checkpoint kinase 1; CO-FISH, chromosome orientation FISH; DDR, DNA damage response; DSB, double-strand break; ES, embryonic stem; HDAC, histone deacetylase; HR, homologous recombination; HU, hydroxyurea; IR, ionizing radiation; MMS, methyl-methane sulfonate; Q-FISH, quantitative FISH; SMC1, structural maintenance of chromosomes 1; TSA, trichostatin A; T-SCE, telomeric sister chromatid exchange.

The online version of this article contains supplemental material.

The Journal of Cell Biology, Vol. 178, No. 7, September 24, 2007 1101–1108
http://www.jcb.org/cgi/doi/10.1083/jcb.200704140

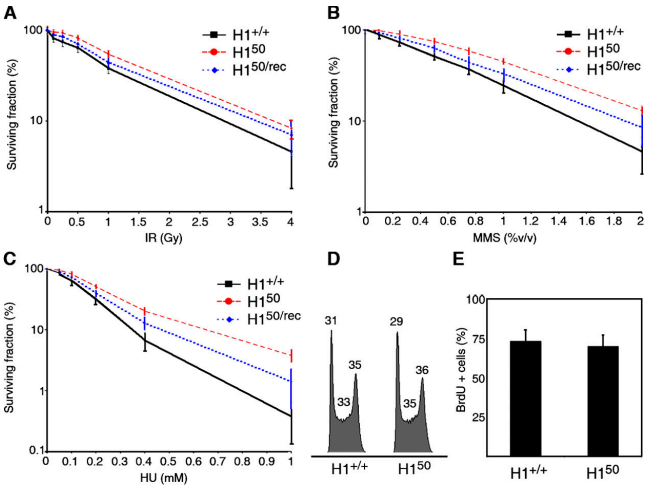

Figure 1. **Reduced H1 levels lead to enhanced resistance to DNA-damaging agents.** Colony-survival assay of $H1^{+/+}$, $H1^{50}$, and $H1^{50/rec}$ ES lines showing the relative surviving fraction of cells exposed to IR (A), MMS (1-h exposure; B), or HU (4-h exposure; C). Data points denote means of three independent experiments performed in triplicate. (D) Cell cycle profiles of $H1^{+/+}$ and $H1^{50}$ ES cells. Numbers indicate the percentage at each cell cycle stage (G1, S, and G2). (E) Percentage of BrdU-positive cells in both genotypes after the same period of BrdU exposure as the one used for HU treatments in C. Error bars represent ±SD.

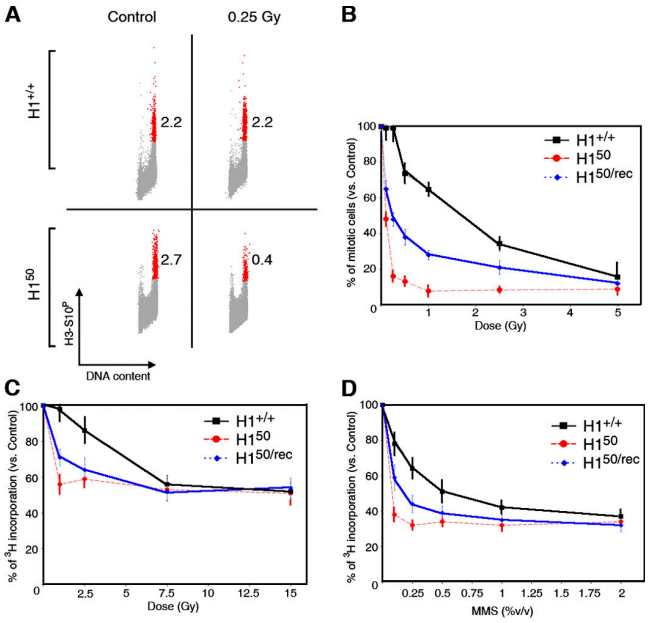

Figure 2. **Hyperactive checkpoint responses in ES cells with reduced levels of H1.** (A) Cell cycle distribution of $H1^{+/+}$ and $H1^{50}$ ES cells before (control) and 1 h after treatment with 0.25 Gy. Propidium iodide staining (x axis) and H3-S10 phosphorylation (y axis) is used to distinguish mitotic (red) from G2 cells. The percentage of mitotic cells is shown for each case. (B) Percentage of mitotic cells (normalized to untreated cells) after exposure to several doses of IR was measured in $H1^{+/+}$, $H1^{50}$, and $H1^{50/rec}$ ES cells as described in A. (C and D) Intra–S phase checkpoint activation in $H1^{+/+}$, $H1^{50}$, and $H1^{50/rec}$ ES cells exposed to increasing doses of IR (C) or MMS (D). Error bars show mean ± SD.

the normal amount of H1 could be obtained. Analysis of these lines showed that the reduction in histone H1 is indeed associated with a less compact chromatin (Fan et al., 2005). Taking advantage of this genetic system, we investigated the competence of the mutant cells in establishing a DDR in the context of a more "open" chromatin configuration.

Results and discussion

To get a general view of how H1-depleted ES cells respond to DSBs, we analyzed the behavior of mutant and control cells in colony-survival assays after a brief exposure to various genotoxic agents (Fig. 1). Regardless of the source, mutant cells were consistently found to be more resistant to DNA damage than their wild-type counterparts, this being more pronounced in the case of alkylating agents such as methyl-methane sulfonate (MMS) than in response to ionizing radiation (IR). Interestingly, $H1^{50}$ ES cells also exhibited resistance to hydroxyurea (HU), which activates the DDR in replicating cells, and this behavior could not be attributed to the difference in the rates of replication between both genotypes (Fig. 1, D and E). In all cases, partial reconstitution of H1-depleted cells with exogenous H1 ($H1^{50/rec}$; Fig. S1, A and B, available at http://www.jcb.org/cgi/content/full/jcb.200704140/DC1) led to an intermediate phenotype in the survival rate. Thus, diminishing the levels of the linker histone H1 renders ES cells hyperresistant to DNA damage.

The better performance of the H1-depleted cells in colony-survival assays is reflective of an enhanced cellular response to DSBs, which in eukaryotes is coordinated by a phosphorylation-based transduction cascade known as the DDR. Beyond individual phosphorylation events, cell cycle checkpoints can be used to measure the output of the DDR. Whereas wild-type ($H1^{+/+}$) and $H1^{50}$ cells arrested similarly on exposure to high doses of radiation, the response to low doses differed substantially among the two genotypes (Fig. 2). A detailed analysis showed that mutant cells activated the G2/M checkpoint at doses in which the cell cycle progression of the wild-type cells remained unaltered (Fig. 2 A). The mutant cells also maintained a more robust response overall (Fig. 2 B). The performance of $H1^{+/+}$ and $H1^{50}$ cells in the intra–S phase checkpoint assay was analogous to that of the G2 arrest, showing an enhanced checkpoint response in the mutant cells (Fig. 2, C and D). Again, the performance of $H1^{50/rec}$ ES cells was found to be intermediate in all cases. Thus, lowering the level of H1 results in an enhanced DDR as measured by the cell cycle arrest induced by DNA damage.

The presence of the "hypercheckpoint" phenotype led us to evaluate the signaling cascade involved in the activation of the arrest. To this extent, and because of its cell cycle–restricted role in the activation of intra–S and G2 checkpoint responses (Zhao et al., 2002), we analyzed the dynamics of chaperoning checkpoint kinase 1 (Chk1) phosphorylation induced by DNA damage. Consistent with the checkpoint data, the levels of $Chk1^{S345P}$ in response to IR were found to be increased in $H1^{50}$ cells at all doses examined, being detectable at doses in which the levels of $Chk1^{S345P}$ in the wild-type cells were not considerably higher than those of untreated cells (Fig. 3, A and B). Similar observations were made in cells treated with HU or MMS (Fig. 3, D–G). In contrast to the Chk1 phosphorylation performed by the ataxia telangiectasia mutated (ATM) and Rad3 related (ATR) even in response to IR (Cuadrado et al., 2006; Jazayeri et al., 2006), the strength of ATM signaling was not affected

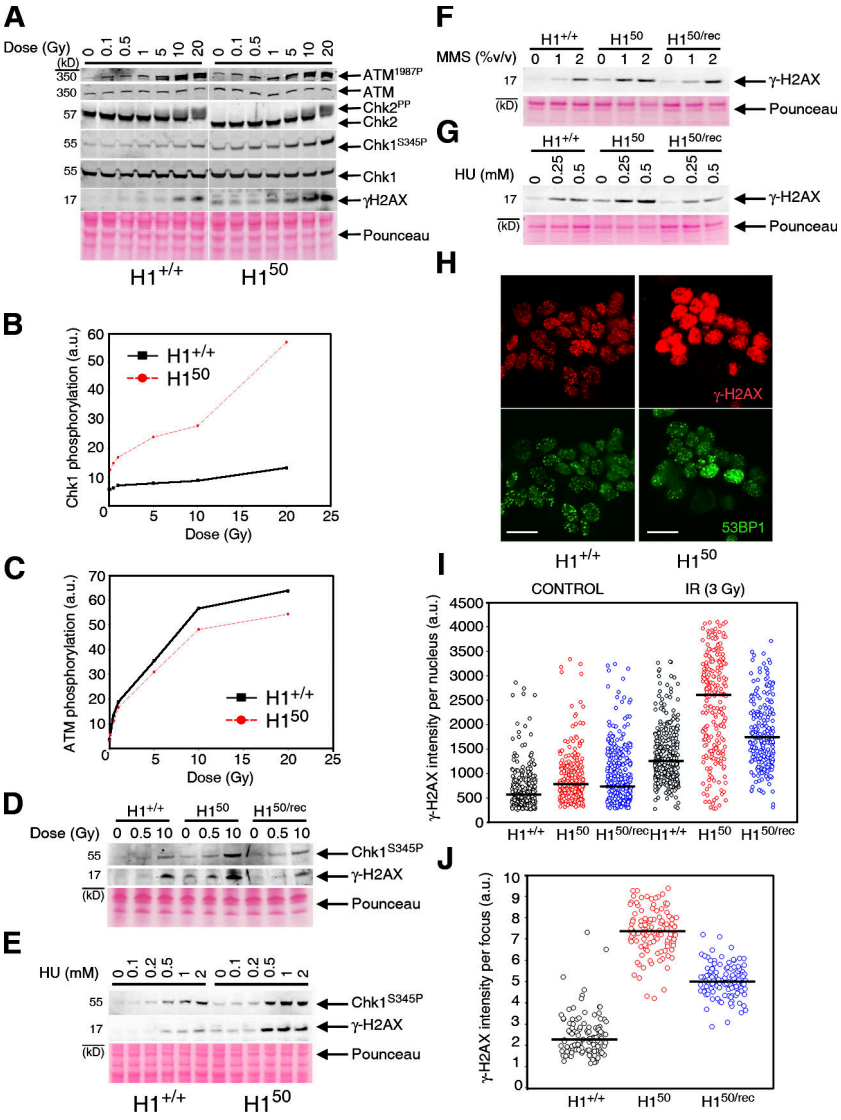

Figure 3. **Enhanced signaling per DSB in H1^{50} cells.** (A) ATM, Chk2, Chk1, and H2AX phosphorylation were analyzed by Western blotting in H1$^{+/+}$ and H1^{50} ES cells exposed to increasing doses of IR. Quantification of Chk1 (B) and ATM (C) phosphorylation from the data observed in A. Data were normalized by total Chk1 and ATM levels, respectively. (D) IR-induced phosphorylation of H2AX and Chk1 in the different genotypes. (E) Chk1 and H2AX phosphorylation in H1$^{+/+}$ and H1^{50} ES cells exposed to increasing doses of HU. MMS- (F) or HU (G)-induced γ-H2AX formation of H1$^{+/+}$, H1^{50}, and H1$^{50/rec}$ ES cells. (H) γ-H2AX (red) and 53BP1 (green) foci analyzed in H1$^{+/+}$ and H1^{50} cells 45 min after exposure to 3 Gy. Bars, 50 μm. (I) Distribution of the γ-H2AX intensity per nucleus in control and irradiated populations of the different genotypes obtained by high-throughput microscopy. Black bars mark median values. (J) Quantification of the amount (integrated intensity) of γ-H2AX present per individual focus.

by H1 levels. These findings are in agreement with the colony survival data, in which the resistance to genotoxicity was more profound in the case of drugs that preferentially activate ATR, such as HU or MMS, than in the case of IR. Nevertheless, an ATR/Chk1-dependent DDR also operates in IR-induced responses (Cuadrado et al., 2006; Jazayeri et al., 2006), and impairment of ATR activity radiosensitizes human cells (Cliby et al., 1998; Wright et al., 1998). Moreover, both the radiosensitivity and G2/M checkpoint defect of ATM-deficient human cells can be rescued by ectopic expression of yeast Chk1 (Chen et al., 1999), demonstrating that a hyperactive ATR pathway is sufficient to stimulate checkpoint signaling and radioresistance in an ATM-independent manner.

Interestingly, phosphorylated H2AX (γ-H2AX) was also found to be increased in the mutant cells in the same conditions, and both Chk1 and H2AX phosphorylation were dampened by H1 reconstitution (Fig. 3 D). The increased γ-H2AX formation could be the consequence of either increased damage being generated at the same doses or of more signaling being generated per individual DSBs. In any case, the resistance to DNA damage will be contradictory with higher amounts of DSBs being formed in the H1^{50} cells. Consistently, neither neutral comet analyses (Fig. S1, C and D) nor the quantification of the number of 53 binding protein 1 (BP1) and γ-H2AX foci that were generated by IR (Fig. S1, E and F) showed substantial differences between the amounts of DSBs generated in H1$^{+/+}$ or H1^{50} ES cells. Of note, the same number of DSBs led to higher endogenous levels of γ-H2AX in replicating cells, which even if not sufficient to have an impact on cell cycle progression might prime the DDR. To evaluate the activation of the DDR at each lesion, we analyzed the distribution of 53BP1 and γ-H2AX foci in response to IR (Fig. 3 H). Consistent with the biochemical data, high-throughput image analysis showed that the mean intensity of γ-H2AX per nucleus was markedly higher in H1-depleted cells (Fig. 3 I). Furthermore, the amount of γ-H2AX per individual focus was found to be markedly higher in H1^{50} than in H1$^{+/+}$ cells (Fig. 3 J), and both phenotypes were partially suppressed in H1$^{50/rec}$ cells. In summary, the hyperactive DDR found in the H1-depleted cells is caused by enhanced signaling that is generated at each individual DSB. In regards to the effect

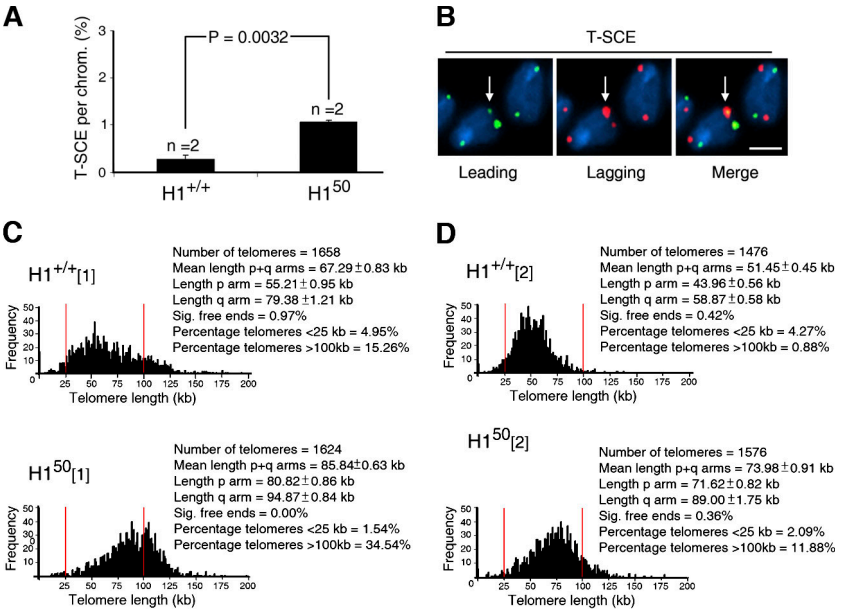

Figure 4. **Increased T-SCE and enlarged telomeres in H1-depleted cells.** (A) Quantification of T-SCE in $H1^{+/+}$ and $H1^{50}$ cells. A significant increase in T-SCE was observed in all cultures of H1-depleted cells (χ^2 test, $P < 0.01$). Error bars correspond to experiments performed in two independent ES lines ($n = 2$). (B) CO-FISH allows for the differential staining of the telomeres coming from the leading (green) or the lagging (red) chromatid. The image illustrates a typical T-SCE event (arrow) that leads to two telomeric signals per chromosome coming from the same sister chromatid, in contrast to the normal pattern found in the absence of recombination events (right). Bar, 1 μm. (C and D) Telomere length distribution in two independently derived pairs of $H1^{+/+}$ and $H1^{50}$ ES lines as determined by Q-FISH.

of chromatin at the DSBs, kinetic analyses of the recruitment of 53BP1 to IR-induced foci (Fig. S1 E) or to a laser-induced path of DSBs (Fig. S1, G–I) showed that this relocalization was slightly fastened in cells with reduced H1 levels. This suggests that the increased signaling per DSB observed in H1-depleted cells might be stimulated by the enhanced accessibility of DDR factors to the lesion site.

Besides the cells' enhanced signaling per lesion and hyper-checkpoint phenotype, the reduction of H1 levels only led to a moderate impact on the overall resistance of the mutant cells to DNA damage. However, this experiment represents the outcome of one single exposure to exogenous damage and it is therefore possible that the constant presence of a hyperactive DDR would have more acute consequences on the genome of H1-depleted cells. One of the roles of DNA repair is handling the breaks generated during the replication process. These type of DSBs are repaired through homologous recombination (HR) using the sister chromatid as the preferred partner. Instead of looking at an exogenous HR system, we evaluated the endogenous levels of sister chromatid exchange at a locus conserved among all chromosomes, the telomere. The analysis of telomeric sister chromatid exchange (T-SCE) of the $H1^{+/+}$ and $H1^{50}$ lines showed that the frequency of this recombination event was almost four times higher in the mutant lines (Fig. 4, A and B). One of the pathways responsible for the control of telomere length is based on recombination between telomeric sequences. Consequently, mutations that increase telomeric recombination rates (such as murine ES cells deficient in DNA methyltransferases DNMT1 or DNMT3a/b) have been found to lead to elongated telomeres (Gonzalo et al., 2006). We therefore evaluated whether the persistent increase in endogenous T-SCE levels also correlated with an increase in the telomere length of $H1^{50}$ cells. As shown in Fig. 4 (C and D), quantitative FISH (Q-FISH) analysis demonstrated a remarkable increase in the telomere length of H1-depleted cells. Whereas we cannot disprove that telomere length might be also influenced by other factors such as the access of telomerase to its target DNA or telomerase activity per se, our data suggest that the enhanced phosphoinositide 3-kinase–related protein kinase signaling observed at each DSB could be stimulating telomeric recombination events at endogenously occurring sites of telomere damage. In agreement with this concept, spontaneously occurring T-SCE events are substantially diminished by ATM depletion in human cells (Fig. S2, available at http://www.jcb.org/cgi/content/full/jcb.200704140/DC1). In summary, our data demonstrate that decreasing H1 levels lead to a general increase in telomere length, an as of yet unrecognized role for mammalian H1 in the regulation of chromosome structure.

With the exception of a very limited set of genes (Fan et al., 2005), the gene expression profile of wild-type and H1 mutant cells is almost identical, suggesting that the observed differences in the signaling of DSBs are more likely related to the role of H1 in chromatin structure. A more extensive transcriptional study performed confirms the previous findings and, specifically, fails to detect any major transcriptional change in components of the DDR (Fig. S3, available at http://www.jcb.org/cgi/content/full/jcb.200704140/DC1). To further investigate whether a more decondensed chromatin, regardless of H1 levels, would cause similar dynamics at DSB sites, we evaluated the activation of the DDR in cells that had been previously treated with the histone deacetylase (HDAC) inhibitor trichostatin A (TSA). Among the different reagents that affect chromatin compaction, TSA was chosen because it is one of the few chromatin-modifying compounds in which the actual effect on global chromatin compaction has been documented in detail (Toth et al., 2004). Importantly, even though the addition of TSA has been previously reported to activate ATM in the absence of damage (Bakkenist and Kastan, 2003), the doses and exposure times used in this analysis did not lead to any detectable phosphorylation of ATM in nonirradiated cells. Pretreatment of human cells (MCF7) with TSA mimicked the observations previously made in H1-depleted ES cells (Fig. 5, A and D).

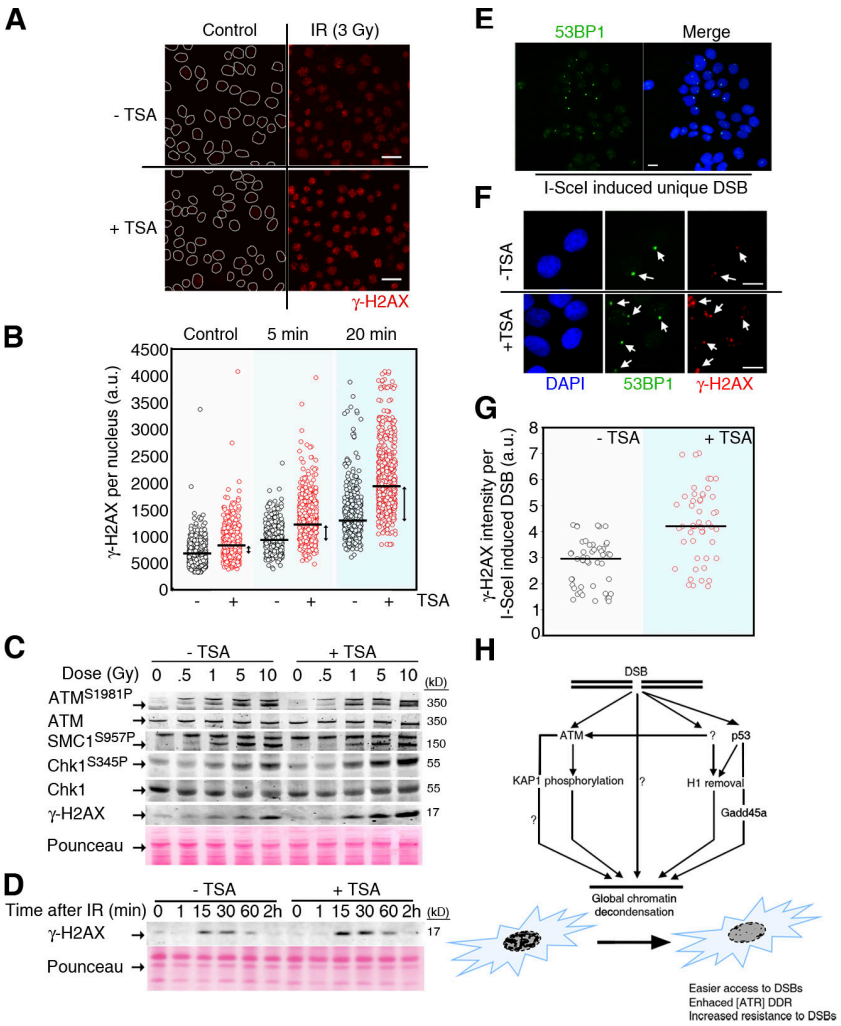

Figure 5. **TSA pretreatment stimulates the DDR.** (A) γ-H2AX foci formation (red) in control or TSA-pretreated MCF7 cells 20 min after exposure to 3 Gy. A white mask shows the location of nuclei (derived from the corresponding DAPI image) in the control cells. TSA treatment was of 0.1 μM for 5 h for all of the experiments shown in this study. Bars, 50 μm. (B) Distribution of the γ-H2AX intensity per nucleus in control and irradiated (3 Gy) populations of untreated or TSA-pretreated MCF7 cells obtained by high-throughput microscopy. Black bars mark median values. Arrows highlight the difference in median intensity between each condition. (C) ATM, SMC1, Chk1, and H2AX phosphorylation was analyzed by Western blotting in control or TSA-pretreated cells 30 min after exposure to several doses of IR. (D) H2AX phosphorylation kinetics in control or TSA-pretreated cells in response to 10 Gy of IR. (E) Representative image showing the pattern of single DSBs induced by I-SceI (as measured by 53BP1 foci) in nuclease-transduced MCF7^{ISceI} cells. (F) Representative image showing 53BP1 and γ-H2AX foci induced by I-SceI (arrows) in nuclease-transduced MCF7^{ISceI} cells either untreated or treated with TSA. 0.1 μM TSA (5 h) was added 24 h after viral transduction. Bars, 20 μm. (G) Quantification of the amount (integrated intensity) of γ-H2AX present per I-SceI–induced focus in control or TSA-pretreated cells was made as described previously (Fig. 3 J and see Materials and methods). (H) Model illustrates the pathways regulating the global chromatin relaxation process induced by DNA damage and how this modulates the outcome of the DDR.

In this manner, TSA pretreatment led to a more robust phosphorylation of Chk1 and H2AX in response to IR without substantially affecting ATM or structural maintenance of chromosomes 1 (SMC1) phosphorylation. Moreover, whereas the amount of 53BP1 foci being generated after IR was not affected by the drug, the signaling emanating from each foci/DSB was higher in TSA-treated cells than in control cells (unpublished data). Equivalent observations were made with other HDAC inhibitors such as sodium butyrate and in several human and murine cell lines (mouse ES, mouse embryonic fibroblast, U2OS, HCT, A549, IMR90, and NIH3T3; unpublished data). Furthermore, the amount of H2AX phosphorylation per individual focus occurring in an I-SceI–transduced MCF7 cell line harboring a unique nuclease recognition site (Fig. 5, E and G) was also found to be enhanced by TSA, formally demonstrating that chromatin condensation limits the signaling strength of each DSB. In summary, both H1 depletion and TSA data support the concept that the strength of the DDR derived from each DSB is modulated by chromatin configuration.

In addition to the use of H1-depleted cells in this model system of open chromatin, our findings on the role of H1 might have functional implications. In fact, the stoichiometry of H1 in higher eukaryotes is nearly one per nucleosome core particle (Woodcock et al., 2006), suggesting that the fine tuning of H1 nucleosome interactions might be an active way of controlling chromatin structure. Several lines of evidence support this notion. For instance, Cdk-mediated phosphorylation of H1 in the S/G2 phases has been shown to weaken the interaction of H1 with chromatin (Roth and Allis, 1992; Dou et al., 1999). In addition, a fraction of the histone H1c variant was shown to leave the nucleus on exposure to DSBs, leading to cytochrome *c* release and activation of apoptosis (Konishi et al., 2003). However, we can also detect H1 removal in mouse embryonic fibroblasts that have only been briefly exposed to the radiomimetic drug neocarzinostatin, supporting additional roles of H1 clearance in the response to DSBs beyond apoptosis (unpublished data). Furthermore, a transient transfection of H1-GFP in MCF7 cells shows that the strength of the DDR is dampened by the overexpression of H1 (Fig. S1 J). Finally, there is evidence that the role of linker histones in modulating the responses to DNA damage might have been established early in evolution. *Saccharomyces cerevisiae* mutants of the *Hho1* linker histone were shown to have increased levels of HR, which was also particularly accentuated at the telomeres (Downs et al., 2003). Because ATM and ATR phosphorylation events also directly stimulate the repair of DSBs (Kuhne et al., 2004; Wang et al., 2004), it will be interesting to

test whether the increased recombination and resistance to MMS found in the yeast strains is also associated with a hyperactive DDR. Beyond its global role in chromatin compaction, the finding of a specific in vivo role for H1 in mammalian cells has remained elusive. Our data on the responses to broken DNA and on the regulation of telomere length now support additional roles for the linker histone H1 in the control of genome architecture.

In this manuscript we have evaluated the precise effect that global chromatin compaction has on the different stages (access, signaling, and repair) of the DDR (Fig. 5 H). Our data suggests that whereas chromatin compaction has a moderate impact on the access and repair of DSBs, it strongly stimulates the signaling of each DNA break. In any case, the differences on repair could be substantial in explaining the damage resistance phenotype. The preferential impact on ATR/Chk1 rather than on ATM/Chk2 might be reflective of the different requirements for chromatin remodeling activities of each pathway. One possibility is that chromatin compaction will limit the resection of each DSB and thus mainly impinge on ATR signaling and HR. Interestingly, the deficiencies in Rad51 loading and HR found in transformation-domain associated protein mutant cells were shown to be reversed by pretreatment with HDAC inhibitors (Rubbi and Milner, 2003; Murr et al., 2006).

The relationship between chromatin and the DDR presented in this study could help to understand the heterogeneity of cellular responses to DNA damage in vivo. For instance, a recent study has shown that $CD133^+$ glioma cancer stem cells show a more robust activation of the DDR that is associated with radioresistance of the tumor-forming population (Bao et al., 2006). Because overall chromatin accessibility is an innate property of stem cells that is lost on differentiation (Meshorer et al., 2006), studying whether the increased DDR of glioma stem cells is just indicative of their chromatin status and thus evaluating whether chromatin compaction might be therapeutically exploited to radiosensitize cancer stem cells should be an interesting avenue for future research.

Materials and methods

Cell lines

Generation of murine ES cells deficient in histone H1c, H1d, and H1e (and quantification of total H1 levels) has been described previously (Fan et al., 2005). Two independently derived pairs of ES cell lines (F18($H1^{+/+}$) and F9($H1^{50}$), and F4($H1^{+/+}$) and F1($H1^{50}$)) at passage numbers 10–12 were used for this study. Generation of $H1^{50/rec}$ cells is described in Fig. S1.

Cell cycle checkpoints

For G2/M checkpoints, cells were mock treated or irradiated, incubated at 37°C for the indicated times, and stained with antibodies recognizing phosphorylated histone H3 (1:50 dilution; Upstate Biotechnology), and the percentage of mitotic cells was quantified by flow cytometry. Intra–S phase checkpoint analyses were performed as described previously (Celeste et al., 2002). In brief, the analysis represents the incorporation of [^{3}H]thymidine in a short pulse after exposure to the genotoxic agent (normalized to the levels of incorporation in the nondamaged cells). In the case of MMS, cells were left with the drug for 45 min before the pulse.

Western blot and immunofluorescence

Primary antibodies used in this work were γ-H2AX and Chk2 (Upstate Biotechnology), 53BP1 and ATM (Novus Biologicals), $Chk1^{S345P}$ (Cell Signaling), Chk1 (Vision BioSystems), $SMC1^{957P}$ (Abcam), ATM^{1981P} (Rockland Immunochemicals, Inc.), and ATM^{1987P} (provided by A. Nussenzweig, National Institutes of Health, Bethesda, MD 20892). For immunofluorescence, secondary antibodies conjugated with Alexa 568 or 488 (Invitrogen) were used at 1:250. For high-throughput microscopy studies, cells were grown on μCLEAR bottom 96-well dishes (Greiner Bio-One) and analyzed with a bioimager (BD Pathway 855; Beckton Dickinson). Image acquisition was performed at room temperature using oil as an immersion media and a camera (ORCA 1394; Hamamatsu Photonics) with a 40× objective (HCX PL APO, 0.75 NA). Image analysis was performed with imaging software (AttoVision; BD Biosciences). The quantification of H2AX intensity per focus was performed with software (Metamorph 7.0; Molecular Devices). All the images for quantitative analyses were acquired under nonsaturating exposure conditions. All Western analyses shown in this study were performed on the LI-COR platform (LI-COR Biosciences) that allows linearly quantitative Western blot with the use of Alexa 680– and 800–conjugated secondary antibodies (Invitrogen).

T-SCE

T-SCE events were measured with the use of chromosome orientation FISH (CO-FISH). In brief, confluent mouse ES cells were subcultured in the presence of BrdU (Sigma-Aldrich) at a final concentration of 10^{-5} M and allowed to replicate their DNA once at 37°C overnight. Colcemid (Sigma-Aldrich) was added at a concentration of 1 μg ml^{-1} for the last hour of incubation. Cells were then recovered and metaphase spreads were prepared as described previously (Samper et al., 2000). CO-FISH was performed as previously described (Bailey et al., 2001), first using a $(TTAGGG)_7$ probe labeled with Cy3 and then a $(CCCTAA)_7$ probe labeled with Rhodamine green (Applied Biosystems). Metaphase spreads were captured on a fluorescence microscope (Leitz DMRB; Leica).

Q-FISH

Metaphase cells were prepared for Q-FISH and hybridized as previously described (Samper et al., 2000). To correct for lamp intensity and alignment, images from fluorescent beads (Invitrogen) were analyzed using the TFL-Telo program (provided by P. Lansdorp, British Columbia Cancer Research Center, Vancouver V5Z 1L3, Canada; Zijlmans et al., 1997). Images and telomere fluorescence values were obtained from at least 10 metaphases for each data point as previously described (Samper et al., 2000).

I-SceI–delivered DSB

Retroviruses producing I-SceI (pMXPIE-ISceI; provided by A. Nussenzweig) were produced in 293 T cells using standard procedures. Retroviral supernanants were then used to transduce a line of MCF7 cells harboring a unique I-SceI site (provided by K.K. Khanna; Queensland Institute of Medical Research, Queensland, Australia). The presence of a considerable population of cells harboring a single DSB was first observed 12 h after transduction and was maximum at day 2 (with ∼60% of the cells containing a single 53BP1 focus).

Generation and analysis of clones expressing exogenous H1

A plasmid (pEBB-H1dHA) that directs expression of H1d under control of the elongation factor 1 α promoter was constructed by inserting an 804-bp PCR DNA fragment including the H1d coding sequence with an HA tag sequence. 10 μg pEBB-H1dHA was cotransfected with 100 ng pcDNA 6/TR (Invitrogen) into 5×10^6 $H1^{50}$ ES cells that were prepared without feeder cells, using the mouse ES cell nucleofector kit (Amaxa) according to the manufacturer's instructions. 2 d after transfection, selection with 10 μg/ml blasticidin was initiated, and single colonies were isolated 11 d later. Clones were propagated in the presence of blasticidin and screened by immunoblotting with an anti-HA antibody (Santa Cruz Biotechnology, Inc.). Total histones were prepared from $\sim 10^7$ cells of the highest expressing clones and analyzed by high-performance liquid chromatography as described previously (Fan et al., 2005) to quantify the level of the exogenous H1d protein. There was no detectable difference in elution times of the exogenous HA-tagged H1d and endogenous H1d.

Comet assay

The neutral comet assay was performed with the Comet assay kit (Trevigen) according to the manufacturer's instructions.

Laser-generated DSBs

53BP1-GFP–transfected ES cells were plated onto a gelatinized black μCLEAR bottom 96-well plates (Greiner Bio-One). The DNA intercalating dye Hoechst 33258 was added at 10 μg/ml and incubated for 20 min at 37°C. The plate was mounted on a microscope stage of a confocal microscope (TCS-SP2; Leica), and cells were irradiated with a 351-nm laser along a user-defined path to generate localized DSBs.

ATM depletion

Retroviral constructs (pRETRO.SUPER backbone) containing control or ATM short hairpin RNAs were provided by Y. Shiloh (Tel Aviv University, Tel Aviv, Israel). Retroviral transduction of HCT116 cells was performed by standard infection procedures. Cells were selected in 2 mg/ml of puromycin for 3 d 24 h after infection.

Transcriptional profiling

Total RNA was extracted from $H1^{+/+}$ and $H1^{50}$ ES cells using the RNeasy midi kit (QIAGEN). Quality of the RNA was determined with a bioanalyzer (2100; Agilent Technologies) and the amount of RNA was established using a spectrophotometer (NanoDrop). RNA amplification and labeling was performed by using the Low RNA input linear amplification kit PLUS (two-color; Agilent Technologies). We used 4 × 44K mouse 60-mer oligo microarray slides (Agilent Technologies) containing four arrays, each with more than 41,000 unique mouse genes and transcripts represented, all with public domain annotations. All procedures of hybridization and slide and image processing were performed according to the manufacturer's instructions (two-color microarray-based gene expression analysis protocol). To account for biases in dye incorporation, dye-swap experiments were performed independently for each comparison; 825 ng of contrasting complementary RNA samples were fragmented at 60°C for 30 min and hybridized at 65°C for 17 h. The slides were then sequentially washed, dried, and scanned at a resolution of 5 μm with a DNA microarray scanner (G2565BA; Agilent Technologies). Signal quantification and data normalization were performed with software (Feature Extraction 9.1; Agilent Technologies) using default analysis parameters for 4 × 44K gene expression arrays (feature extraction protocol GE2-v5_91_0806). The assay was performed in duplicates with dye-swapping to compensate for labeling biases. The entire dataset can be found in Table S1.

H1 transfection

10 μg H1-GFP (provided by T. Misteli, National Institutes of Health) was transiently transfected in MCF7 cells using Lipofectamine 2000 (Invitrogen). After 24 h of transfection, cells were seeded onto black μCLEAR bottom 96-well plates for irradiation and high-throughput microscopy studies (see Western blot and immunofluorescence).

Online supplemental material

Fig. S1 contains additional datasets regarding the role of H1 on the DDR. Fig. S2 shows the role of ATM on the regulation of telomere recombination. Fig. S3 contains an overview of the transcriptome analyses of $H1^{+/+}$ and $H1^{50}$ cells. Table S1 contains the entire dataset of the microarray analyses shown in Fig. S3. Online supplemental material is available at http://www.jcb.org/cgi/content/full/jcb.200704140/DC1.

We thank Dr. J. Mendez for critical comments on the manuscript.

M. Murga is supported by a Ramón y Cajal contract from the Spanish Ministry of Science and Education (RYC-20040002731) and from a grant from Fondo de Investigaciones Sanitarias (PI05945). Work in O. Fernandez-Capetillo's laboratory is supported by grants from the Spanish Ministry of Science (RYC-2003-003610 and BFU2005-09429/BMC), Swiss Bridge (Swiss Bridge Award 2005), and Epigenome Network of Excellence (EU-FP6). Y. Fan and A. Skoultchi were supported by National Institutes of Health grant CA79057.

Submitted: 24 April 2007
Accepted: 20 August 2007

References

Bailey, S.M., M.N. Cornforth, A. Kurimasa, D.J. Chen, and E.H. Goodwin. 2001. Strand-specific postreplicative processing of mammalian telomeres. *Science*. 293:2462–2465.

Bakkenist, C.J., and M.B. Kastan. 2003. DNA damage activates ATM through intermolecular autophosphorylation and dimer dissociation. *Nature*. 421:499–506.

Bao, S., Q. Wu, R.E. McLendon, Y. Hao, Q. Shi, A.B. Hjelmeland, M.W. Dewhirst, D.D. Bigner, and J.N. Rich. 2006. Glioma stem cells promote radioresistance by preferential activation of the DNA damage response. *Nature*. 444:756–760.

Carrier, F., P.T. Georgel, P. Pourquier, M. Blake, H.U. Kontny, M.J. Antinore, M. Gariboldi, T.G. Myers, J.N. Weinstein, Y. Pommier, and A.J. Fornace Jr. 1999. Gadd45, a p53-responsive stress protein, modifies DNA accessibility on damaged chromatin. *Mol. Cell. Biol.* 19:1673–1685.

Celeste, A., S. Petersen, P.J. Romanienko, O. Fernandez-Capetillo, H.T. Chen, O.A. Sedelnikova, B. Reina-San-Martin, V. Coppola, E. Meffre, M.J. Difilippantonio, et al. 2002. Genomic instability in mice lacking histone H2AX. *Science*. 296:922–927.

Chen, P., M. Gatei, M.J. O'Connell, K.K. Khanna, S.J. Bugg, A. Hogg, S.P. Scott, K. Hobson, and M.F. Lavin. 1999. Chk1 complements the G2/M checkpoint defect and radiosensitivity of ataxia-telangiectasia cells. *Oncogene*. 18:249–256.

Cliby, W.A., C.J. Roberts, K.A. Cimprich, C.M. Stringer, J.R. Lamb, S.L. Schreiber, and S.H. Friend. 1998. Overexpression of a kinase-inactive ATR protein causes sensitivity to DNA-damaging agents and defects in cell cycle checkpoints. *EMBO J.* 17:159–169.

Cuadrado, M., B. Martinez-Pastor, M. Murga, L.I. Toledo, P. Gutierrez-Martinez, E. Lopez, and O. Fernandez-Capetillo. 2006. ATM regulates ATR chromatin loading in response to DNA double-strand breaks. *J. Exp. Med.* 203:297–303.

Dou, Y., C.A. Mizzen, M. Abrams, C.D. Allis, and M.A. Gorovsky. 1999. Phosphorylation of linker histone H1 regulates gene expression in vivo by mimicking H1 removal. *Mol. Cell*. 4:641–647.

Downs, J.A., E. Kosmidou, A. Morgan, and S.P. Jackson. 2003. Suppression of homologous recombination by the *Saccharomyces cerevisiae* linker histone. *Mol. Cell*. 11:1685–1692.

Fan, Y., T. Nikitina, E.M. Morin-Kensicki, J. Zhao, T.R. Magnuson, C.L. Woodcock, and A.I. Skoultchi. 2003. H1 linker histones are essential for mouse development and affect nucleosome spacing in vivo. *Mol. Cell. Biol.* 23:4559–4572.

Fan, Y., T. Nikitina, J. Zhao, T.J. Fleury, R. Bhattacharyya, E.E. Bouhassira, A. Stein, C.L. Woodcock, and A.I. Skoultchi. 2005. Histone H1 depletion in mammals alters global chromatin structure but causes specific changes in gene regulation. *Cell*. 123:1199–1212.

Fernandez-Capetillo, O., A. Lee, M. Nussenzweig, and A. Nussenzweig. 2004. H2AX: the histone guardian of the genome. *DNA Repair (Amst.)*. 3:959–967.

Gonzalo, S., I. Jaco, M.F. Fraga, T. Chen, E. Li, M. Esteller, and M.A. Blasco. 2006. DNA methyltransferases control telomere length and telomere recombination in mammalian cells. *Nat. Cell Biol.* 8:416–424.

Jazayeri, A., J. Falck, C. Lukas, J. Bartek, G.C. Smith, J. Lukas, and S.P. Jackson. 2006. ATM- and cell cycle-dependent regulation of ATR in response to DNA double-strand breaks. *Nat. Cell Biol.* 8:37–45.

Konishi, A., S. Shimizu, J. Hirota, T. Takao, Y. Fan, Y. Matsuoka, L. Zhang, Y. Yoneda, Y. Fujii, A.I. Skoultchi, and Y. Tsujimoto. 2003. Involvement of histone H1.2 in apoptosis induced by DNA double-strand breaks. *Cell*. 114:673–688.

Kuhne, M., E. Riballo, N. Rief, K. Rothkamm, P.A. Jeggo, and M. Lobrich. 2004. A double-strand break repair defect in ATM-deficient cells contributes to radiosensitivity. *Cancer Res.* 64:500–508.

Meshorer, E., D. Yellajoshula, E. George, P.J. Scambler, D.T. Brown, and T. Misteli. 2006. Hyperdynamic plasticity of chromatin proteins in pluripotent embryonic stem cells. *Dev. Cell*. 10:105–116.

Murr, R., J.I. Loizou, Y.G. Yang, C. Cuenin, H. Li, Z.Q. Wang, and Z. Herceg. 2006. Histone acetylation by Trrap-Tip60 modulates loading of repair proteins and repair of DNA double-strand breaks. *Nat. Cell Biol.* 8:91–99.

Rogakou, E.P., D.R. Pilch, A.H. Orr, V.S. Ivanova, and W.M. Bonner. 1998. DNA double-stranded breaks induce histone H2AX phosphorylation on serine 139. *J. Biol. Chem.* 273:5858–5868.

Roth, S.Y., and C.D. Allis. 1992. Chromatin condensation: does histone H1 dephosphorylation play a role? *Trends Biochem. Sci.* 17:93–98.

Rubbi, C.P., and J. Milner. 2003. p53 is a chromatin accessibility factor for nucleotide excision repair of DNA damage. *EMBO J.* 22:975–986.

Samper, E., F.A. Goytisolo, P. Slijepcevic, P.P. van Buul, and M.A. Blasco. 2000. Mammalian Ku86 protein prevents telomeric fusions independently of the length of TTAGGG repeats and the G-strand overhang. *EMBO Rep.* 1:244–252.

Takahashi, K., and I. Kaneko. 1985. Changes in nuclease sensitivity of mammalian cells after irradiation with 60Co gamma-rays. *Int. J. Radiat. Biol. Relat. Stud. Phys. Chem. Med.* 48:389–395.

Toth, K.F., T.A. Knoch, M. Wachsmuth, M. Frank-Stohr, M. Stohr, C.P. Bacher, G. Muller, and K. Rippe. 2004. Trichostatin A-induced histone acetylation causes decondensation of interphase chromatin. *J. Cell Sci.* 117:4277–4287.

Wang, H., S.N. Powell, G. Iliakis, and Y. Wang. 2004. ATR affecting cell radiosensitivity is dependent on homologous recombination repair but independent of nonhomologous end joining. *Cancer Res.* 64:7139–7143.

Woodcock, C.L., A.I. Skoultchi, and Y. Fan. 2006. Role of linker histone in chromatin structure and function: H1 stoichiometry and nucleosome repeat length. *Chromosome Res.* 14:17–25.

Wright, J.A., K.S. Keegan, D.R. Herendeen, N.J. Bentley, A.M. Carr, M.F. Hoekstra, and P. Concannon. 1998. Protein kinase mutants of human ATR increase sensitivity to UV and ionizing radiation and abrogate cell cycle checkpoint control. *Proc. Natl. Acad. Sci. USA*. 95:7445–7450.

Zhao, H., J.L. Watkins, and H. Piwnica-Worms. 2002. Disruption of the checkpoint kinase 1/cell division cycle 25A pathway abrogates ionizing radiation-induced S and G2 checkpoints. *Proc. Natl. Acad. Sci. USA*. 99:14795–14800.

Zijlmans, J.M., U.M. Martens, S.S. Poon, A.K. Raap, H.J. Tanke, R.K. Ward, and P.M. Lansdorp. 1997. Telomeres in the mouse have large inter-chromosomal variations in the number of T2AG3 repeats. *Proc. Natl. Acad. Sci. USA*. 94:7423–7428.

Ziv, Y., D. Bielopolski, Y. Galanty, C. Lukas, Y. Taya, D.C. Schultz, J. Lukas, S. Bekker-Jensen, J. Bartek, and Y. Shiloh. 2006. Chromatin relaxation in response to DNA double-strand breaks is modulated by a novel ATM- and KAP-1 dependent pathway. *Nat. Cell Biol.* 8:870–876.